Organic & Biomolecular Chemistry

Accepted Manuscript

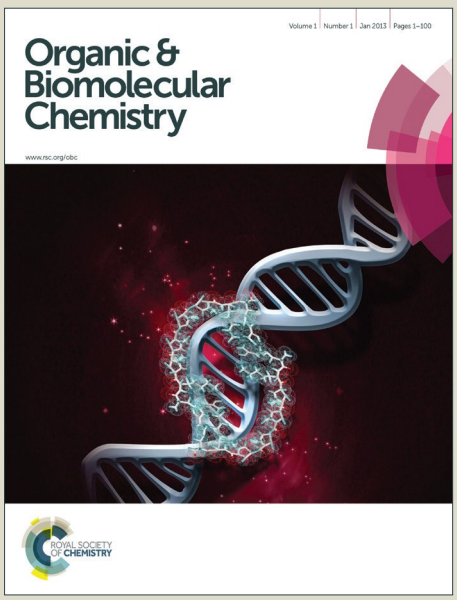

ROYAL SOCIETY OF CHEMISTRY

www.rsc.org/obc

Journal Name

ARTICLE

Targeting Tumor Hypoxia: A Third Generation 2-Nitroimidazole–Indocyanine Dye–Conjugate with Improved Fluorescent Yield

Received 00th January 20xx,
Accepted 00th January 20xx

DOI: 10.1039/x0xx00000x

www.rsc.org/

Feifei Zhou,[1a] Saeid Zanganeh,[1a] Innus Mohammad,[2a] Christopher Dietz,[2a] Akram Abuteen,[1] Michael B. Smith,*[2] Quing Zhu*[1]

Tumor hypoxia is associated with the rapid proliferation and growth of malignant tumors, and the ability to detect tumor hypoxia is important for predicting tumor response to anti-cancer treatments. We have developed a class of dye-conjugates that are related to indocyanine green (ICG, **1**) to target tumor hypoxia, based on *in vivo* infrared fluorescence imaging using nitroimidazole moieties linked to indocyanine fluorescent dyes. We previously reported that linking 2-nitroimidazole to an indocyanine dicarboxylic acid dye derivative (**2**) using an ethanolamine linker (ethanolamine-2-nitroimidazole-ICG, **3**), led to a dye-conjugate that gave promising results for targeting cancer hypoxia *in vivo*. Structural modification of the dye conjugate replaced the ethanolamine unit with a piperazineacetyl unit and led a second generation dye conjugate, piperzine-2-nitroimidazole-ICG (**4**). This second generation dye-conjugate showed improved targeting of tumor hypoxia when compared with **3**. Based on the hypothesis that molecules with more planar and rigid structures have a higher fluorescence yield, as they could release less absorbed energy through molecular vibration or collision, we have developed a new 2-nitroimidazole ICG conjugate, **12**, with two carbon atoms less in the polyene linker. Dye-conjugate **12** was prepared from our new dye (**8**), and coupled to 2-nitroimidazole using a piperazine linker to produce this third-generation dye-conjugate. Spectral measurements showed that the absorption/emission wavelengths of 657/670 were shifted ~100 nm from the second-generation hypoxia dye of 755/780 nm. Its fluorescence quantum yield was measured to be 0.467, which is about 5 times higher than that of **4** (0.083). *In vivo* experiments were conducted with balb/c mice and **12** showed more than twice the average *in vivo* fluorescence intensity in the tumor beyond two hours post retro-orbital injection as compared with **4**. These initial results suggest that **12** may significantly improve *in vivo* tumor hypoxia targeting.

Introduction

Tumor hypoxia mainly appears as a structural or functional misbalance between the tumor micro-environmental

[a]Equal contribution. [1] Department of Biomedical Engineering and Electrical Engineering, University of Connecticut, Storrs, CT, USA. [2] Department of Chemistry, University of Connecticut, Storrs CT, USA
* Communicating authors: MBS, michael.smith@uconn.edu; QZ, zhu@engr.uconn.edu

oxygen supply and consumption, and is associated with the rapid progression of malignant tumors.[1,2,3,4] The identification of tumor hypoxia is important for the assessment and prediction of therapy, because it is known to cause an aggressive phenotype and is associated with an increased resistance to therapy.[5,6] Positron emission tomography (PET) is an established method for imaging hypoxia noninvasively.[7] Imidazole compounds are widely used to prepare PET radionuclides, and it is known that 2-nitroimidazoles show an affinity for hypoxic cells, with the highest electron affinities of this class of compounds.[8,9 ,10,11,12] There are problems associated with PET, including the requirement that radioactive tracer must be administered to patients by injection, as well as the high system cost. Such problems have spurred the development of alternative tumor hypoxia imaging techniques.

Indocyanine green (ICG, **1** in Figure 1) is the only FDA approved fluorescence imaging agent for patient use, but its application is hindered by the problems of a low quantum yield and quick loss of fluorescence after binding to proteins in circulating blood.[13,14,15] In previous work, we demonstrated a noninvasive method for *in vivo* imaging of hypoxic tumors.[16] This method is based on fluorescence infrared imaging of dyes in hypoxic tumors, after injection of a nitroimidazole-indocyanine dicarboxylic acid conjugate, henceforth referred to as a dye-conjugate. In that work, dicarboxylic acid **2** was used as the untargeted dye rather than **1**, and 2-nitroimidazole was linked to the dye using ethanolamine[17,16] or piperazine[18] linkers as shown in Figure 1. We thus prepared hypoxia targeting ethanolamine-dye conjugate **3** and a piperazine-dye conjugate **4**, both linked to 2-nitroimidazole moieties.

Our first-generation dye conjugate (**3**) was shown to be a successful candidate for noninvasive tumor hypoxia mapping using a near-infrared fluorescence imaging technique.[17] The fluorescence signals were measured to be two-fold higher at the

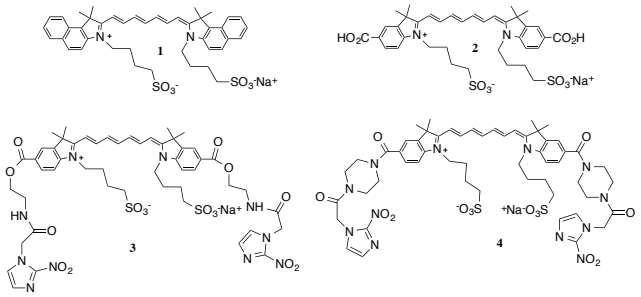

Figure 1. Indocyanine dyes and first and second-generation dye conjugates

tumor site, relative to the untargeted dye **2**.[19] Furthermore, we showed that **3** could be detected in the tumor for 5-7 h, post-injection. We viewed the ester linkage in **3** as too labile and in an effort to improve in vivo efficacy we replaced the ethanolamine moiety with a more robust piperazine moiety, generating the second-generation dye conjugate **4**.[18] In *vivo* targeting experiments in mice with **4** showed a two-fold higher fluorescence in hypoxic tumors relative to **3**, within three h of injection, and the fluorescence was 1.6-1.7 times higher beyond three h.[18]

Further research in our laboratories has focused on improving the fluorescent yield of the dye, in an effort to improve *in vivo* detectability and/or to allow diminished dosing. It is known that molecules with more planar and rigid structures have a higher fluorescence yield as they release less absorbed energy via molecular vibration or collision.[20,21] Based on this hypothesis, we examined structural changes in the dye (**2**). We found that introduction of a ring into the polyene unit of **2** led to a lower fluorescent yield,[22] but shortening the polyene chain by two carbon atoms (see **8** in Scheme 1) led to significant enhancement in fluorescence (see Table 1).

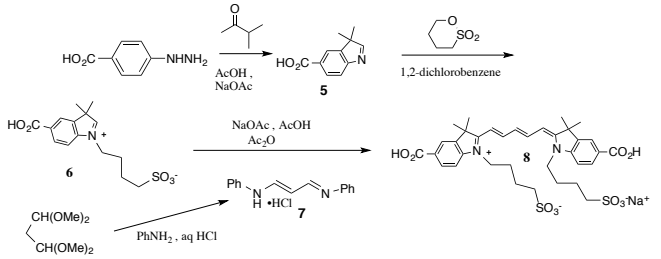

Scheme 1. Synthesis of rigid dye **8**.

With our new dye, **8**, in hand, we synthesized a third generation 2-nitroimidazole ICG conjugate (**12** in Scheme 2), the hypoxia-targeted rigid dye in subsequent figures. The bis(carboxylic acids) **2** and **8** are referred to as non-targeted dyes because they do not have the nitroimidazole moiety associated with targeting tumor hypoxia. The goal of this study is to quantify the *in vivo* hypoxia targeting capability of **12** relative to the non-targeted dyes as well as relative to **4**, using a murine tumor model. A direct comparison of the *in vivo* performance of the rigid dye-conjugate **12** with the second-generation hypoxia-targeting dye (**4**) showed greatly improved imaging for **12**. The biodistribution of each dye in different organs was also evaluated and compared with fluorescence peak intensity of the dye in the tumor.

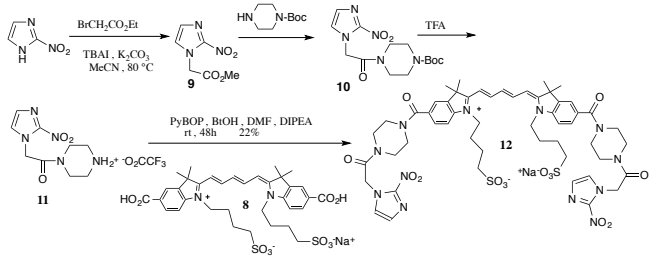

Scheme 2. Synthesis of third generation dye-conjugate **12**.

Results

Optical properties of dyes

The optical properties of **12** were measured and are shown in Figure 2. The absorption maximum for **12** was at 657 nm and the emission maximum was at 670 nm, a shift of around 100 nm and 110 nm for absorption and emission, respectively, when compared with **4**. The other measured optical properties for non-targeted rigid dye **8** and hypoxia-targeted rigid dye **12** in 9.25% sucrose solvent are shown in Table 1.

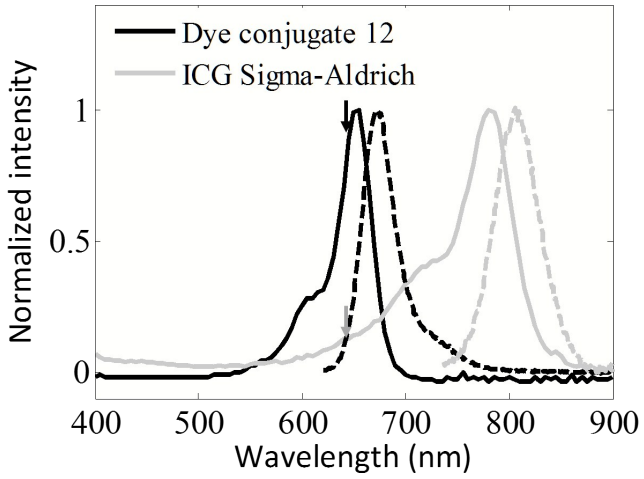

Figure 2. Normalized absorption (solid curves) and fluorescence (dash curves) spectra of hypoxia-targeted rigid dye **12** (black) and ICG from Sigma-Aldrich (gray). This figure shows that in measuring the quantum yield with the standard dye of ICG from Sigma-Aldrich, the excitation was performed at 640 nm, as labeled with arrows. The fluorescence was collected from 650-900 nm for all dyes. Six concentrations of each dye were measured for the calculation of quantum yield. All dyes are measured with spectrometer gain set at medium and the measurements are performed in 9.25% sucrose. The spectra of non-targeted rigid dye **8** is similar to that of **12**. The spectra of biscarboxylic acid ICG **2** and piperazine-2-nitroimidazole-ICG **4** can be referred from past report.[18]

Table 1. The optical properties of rigid dyes in 9.25% sucrose solution

Compound	$\lambda_{abs}^{max}(nm)$	$\lambda_{ems}^{max}(nm)$	Extinction coefficient ε ($M^{-1}cm^{-1}$)	Quantum yield (Φ)
Non-targeted rigid dye **8**	657	671	261,971	0.403
Hypoxia-targeted rigid dye **12**	657	669	268,006	0.467

The *in vivo* distribution of the Dye-Conjugate as a function of time

Figure 3 shows a typical set of fluorescent images obtained by IVIS Lumina II Imaging System over a 48 hour period for a mouse injected with 100 µl of **2** (a), **4** (b), **8** (c) and **12** (d) at 25 µM concentration. All dyes were accumulated in

and cleared from the tumor area with visible and different washout rates, reflecting tracer-specific uptake mechanisms. The improvement on the fluorescence intensity of dye accumulated in the tumor region after longer washout times is visible in Figure 3.

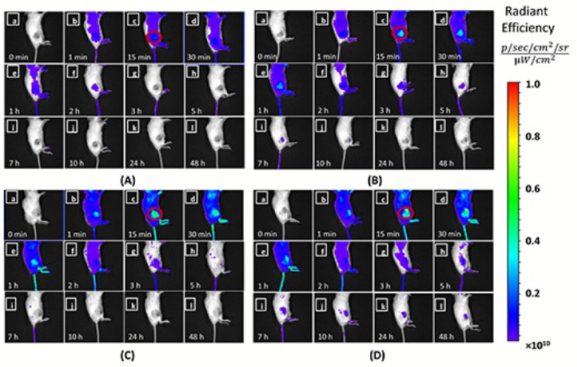

Figure 3. Typical sets of fluorescent images as a function of time. The first row shows fluorescent images obtained by IVIS Lumina II Imaging System using a 710±15 nm/810-875 nm excitation/collection filter pair over a 48 h period for individual mouse injected with 100 μL of (A) ICG **2**; (B) piperazine-2-nitroimidazole-ICG **4**. The second row shows fluorescent images using a 640±15 nm/695-770 nm excitation/collection filter pair over a 48 h period for individual mouse injected with 100 μL of (C) dye **8** and (D) dye **12**. The tumor area for each case was labelled with red circles when the tumor fluorescence intensity reaches to the peak at around 15 min post-injection.

Dye washout characteristics

The washout curves of each dye in tumor area were averaged at each observation point, and the bar plot with standard deviation (STD) for washout period is shown in Fig. 4. The number of mice injected with a particular dye is represented by the parameter *n* in Figure 4. It is shown that for **12** the fluorescence intensity reached an average maximum of 8.0×10^9 (Radiant efficiency, unit: p/sec/cm²/sr/(μW/cm²)) in 5-15 min post-injection and the signal remained above detection level (2×10^8, decided by background fluorescence) in 48 h. For **8**, the fluorescence reached an average maximum of 7.0×10^9 in 5-15 min post-injection and the signal remained above detection level in 10 h. The fluorescence for **4** reached its average maximum intensity of 3.5×10^9 at 15 min and the signal remained above detection level in 10 h. For **2**, fluorescence intensity reached lower average maximum of 1.5×10^9 approximately at 15 min and then the signal was decreased below detection level by around 3 h post-injection.

Two-sided student's t-test was performed between average values of **12** and **8, 12** and **4**, **12** and **2** in the 2-48 h window and results show statistically significance between each pair (Figure 4). Within the 2-48 h time window, the average fluorescence peak intensity of the tumor injected with the hypoxia-targeted rigid dye (**12**) is 2.7 times that of the non-targeted rigid dye (**8**), 1.9 times that of the piperazine-2-nitroimidazole-ICG (**4**), and 7.2 times that of the biscarboxylic acid ICG (**2**).

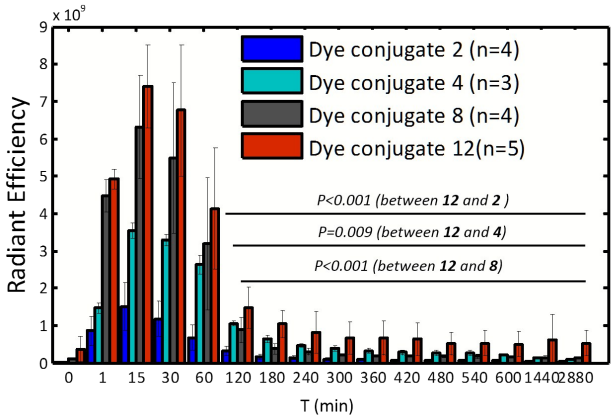

Figure 4. Kinetics of tumor uptake and washout characteristics of hypoxia-targeted rigid dye **12**, non-targeted rigid dye **8**, piperazine-2-nitroimidazole-ICG **4** and biscarboxylic acid ICG **2**. The parameter *n* is the number of mice injected with that dye. All tracers were injected at 25 μM concentration.

Dye residue in tumor after 48 hours

All mice were sacrificed after 48 h post-injection. Tumor tissue were excised and imaged using the same imaging conditions (Figure 5). For mice injected with **2**, an average maximum fluorescence intensity of 0.4×10^8 was detected in the tumor. For mice injected with **4** and **8**, higher averaged maximum fluorescence intensity of 1.5×10^8 and 2.2×10^8, respectively, were detected in the tumor. The highest averaged

maximum fluorescence intensity of tumor was in the group injected with the **12**, measured as 5.0×10^8.

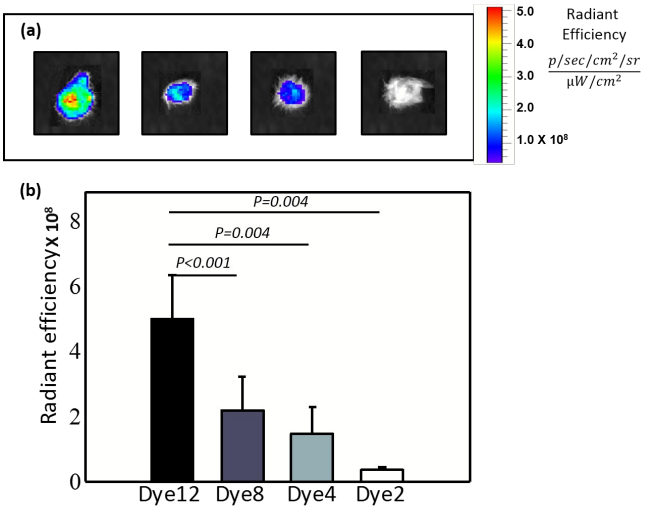

Figure 5. Dye residue in excised tumor tissue. (a) Fluorescence images of excised tumors from tumor bearing mouse injected with 100 µL (from left to right): dye **12**, dye **8,** dye **4**, and dye **2**, all at 25 µM concentration. (b) Statistical results in different groups of mice tumor.

The fluorescence peak intensity of the excised tumor injected with hypoxia-targeted rigid dye (**12**) after 48 hours is about 2.3 times that of the non-targeted rigid dye (**8**), 3.4 times that of the piperazine-2-nitroimidazole-ICG (**4**), and 14 times that of the biscarboxylic acid ICG (**2**). The two-sided student's t-test on the excised tumor radiant efficiency data between hypoxia-targeted (**12**) and non-targeted rigid dye (**8**) is statistically significant (p=0.004).

By comparing the fluorescence radiant efficiency of the dye *in vivo* at 48 h post-injection (Figure 4) and radiant efficiency of the excised tumors (Figure 5), we observed similar or higher fluorescence intensity in the latter (*in vivo*: 5.3×10^8, 1.3×10^8, 9.7×10^7, 2.5×10^7 versus excised tumors*:* 5.0×10^8, 2.2×10^8, 1.5×10^8, 3.5×10^7, for each dye respectively). The imaging was performed on excised tumor without skin, so it is reasonable to expect that the measured dye fluorescence intensity is similar or higher.

Immunohistochemistry (IHC) and dual labeling results

Typical fluorescence images labelled with pimonidazole hydrochloride-FITC (green, channel 2) and with hypoxia-targeted dye **12** and non-targeted rigid dye **8** (red, channel 1), are shown in Figure 6 top and middle row respectively. The targeted rigid dye **12** labelled area is mainly located in the center region and correlates with the region labelled with pimonidazole hydrochloride-FITC; while the non-targeted dye **8** labelled regions are scattered and showed no significant overlap with the region labelled with pimonidazole hydrochloride. On average, the correlation coefficient between channel 1 and channel 2 images of **12** and **8** is statistically significant ($p<0.05$) as shown in Figure 6 (g).

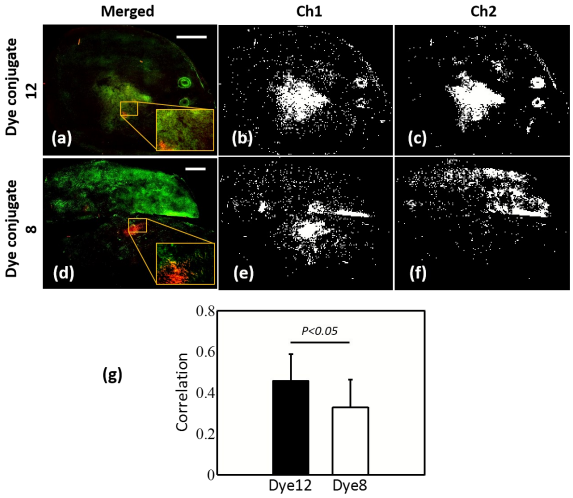

Figure 6. IHC results. Top row: (a) Typical overlaid fluorescence image labelled by dye **12** and commercial pimonidazole hydrochloride. (b) Binary image acquired through microscope channel 1 (Cy5) after processing with 11-12% threshold. (c) Binary image acquired through microscope channel 2 (FITC) after processing. Middle row: (d) Typical overlaid fluorescence image labelled by dye **8** (NT-Rigid) and pimonidazole hydrochloride. (e) Binary image acquired through microscope channel 1 (Cy5) after processing. (f) Binary image acquired through microscope channel 2 (FITC) after processing. The scale bars in (a) and (d) indicate 1 mm. Bottom row: (g) Correlation coefficients computed between Ch1 and Ch2 binary images (hypoxia-targeted rigid dye n=12, non-targeted rigid dye n=8).

Stability of dyes 2, 4, 8, and 12

All dyes in this work were examined *in vivo* over the course of several hours. After each synthesis, and prior to the *in vivo studies*, all dyes were stored in the dark in a refrigerator until a solution of the dye was prepared in PBS as required for the mouse studies. We examined the photostability of dyes **2**, **4**, **8**, and **12** when exposed to light. A solution of each dye in 9.25% sucrose was examined at 750 nm and 650 nm for the ICG and rigid dyes respectively. The initial absorbance data was measured and then every 15 min for the first hour and every hour thereafter. Each sample was irradiated under a 500 W halogen lamp, maintained at a distance of 600 mm, for 15 h. These conditions are rather harsh and certainly more severe than encountered under our experimental studies, but we wanted to understand the relative photostability of these dyes. Our results are shown in Figure 7, which shows that both the parent dye **2** and the second generation dye conjugate **4** decomposed at ambient temperature rather quickly, although each dye persisted for about 3-4 hours. Interestingly, our 'rigid dye' **8** and also the dye-conjugate **12** showed improved photostability, decomposing much more slowly. Indeed, there was a detectable concentration of both dyes after 12 hours. The dye-conjugate **12** showed slightly improved photostability relative to the parent **8**.

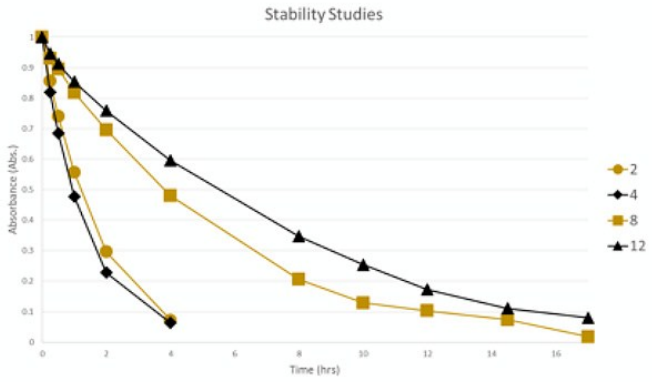

Figure 7. Dye stability study for **2**, **4**, **8**, and **12**.

Discussion

As anticipated, our results show that higher fluorescence intensity is achieved with rigid dye **12** as compared with the second generation dye **4**, although the absorption/emission wavelengths shifted ~100 nm from the second generation dye: from 755/780 nm to 657/670 nm (see Figure 2). The fluorescence quantum yield of rigid dyes was measured to be about 0.4, which is around 5 times higher than that of the second-generation dyes. We believe that the reason for the spectrum shift and quantum yield increase of the rigid dye **8** and the dye-conjugate **12** is due to the more rigid structure of the polyene chain, but the specific structural feature that correlates with these changes is unknown at this time.[22]

Florescence images of the sliced, excised tumor tissue indicate that the dye molecules were not only distributed in tumor periphery area, but also penetrated throughout the entire tumor. Although the specific molecules this probe is binding to are yet to be investigated, from the report of other 2-nitroimidazole conjugated dye studies,[23] we anticipate that this finding is due to the presence of nitroimidazole moiety. It is known that 2-nitroimidazole derivatives are trapped in the cells under hypoxic conditions, and our results are consistent with similar behavior for **4** and **12**.

Despite the high retention of piperazine-2-nitroimidazole-linked dyes **4** and **12** in the tumor region, results also show higher fluorescence intensity in the kidney and liver 48 h post-injection. In general, we observed that urine contained concentrated fluorescence dye. Previous reports indicated that ICG was selectively bound to the liver, later excreted in the bile due to its binding with serum proteins and then eliminated by giving bile to the feces.[24,25] We therefore expect that this soluble dye conjugate is mainly washed out through the kidney and also removed through liver and gall bladder.

Our work suggests that the dye-conjugates are widely distributed in the mouse after injection. However, washout occurs quickly, presumably by excretion, but dye conjugate **12** is retained in the tumor to a significantly greater extent when compared to precursor **8** (see Figure 5). Further, rigid dye **12** is retained in the tumor to a greater extent than **4**. A direct comparison of residual fluorescence intensity of **8** with early versions of hypoxia targeted dye **4** is irrelevant because dye **8** has a 5 times higher quantum yield than that of **4**. The hypoxia targeting related tumor retention (average fluorescence intensive measured between 120-2880 min/ maximum fluorescence intensity) of dye **8** was 0.038, which was much smaller than those of dye **4** and **2** (0.106 and 0.066 respectively).

Our data, presented in Figure 4, indicates that for the same concentration, dye **4** is retained in the tumor to a greater extent than **12** or **8**. This conclusion is based on a comparison of dye intensity in the tumor at > 2 hours post-injection (2-48 h) relative to the maximum intensity observed for each dye (5-15 min). However, both **8** and **12** have a higher fluorescence yield, which makes them easier to detect. This observation suggests that **12** may be used for detection of tumor hypoxia using a significantly lower dose relative to **4**.

The correlation between the dual-channel labelled images was performed after applying a threshold to binary images. By varying the threshold from 8-20%, we found that a lower threshold can cause a large variation among tumor samples due to noise. The best threshold was found to be 11-12%.

A cytotoxicity study is beyond the scope of this current work, but is clearly required if **12** is to be pursued as a useful imaging agent. However, we found no observable difference for the mice groups based on post-injection activity or weight loss, suggesting that no significant short-term toxicity occurred to the mice injected with **12**.

Experimental

Materials

The details of the synthetic procedures used to prepare **2**–**4**, as well as their photophysical/chemical properties in various solutions, have been reported previously.[22,17] We prepared the non-targeted rigid dye, (**8)** with two carbons less in the polyene linker compared to ICG dicarboxylic acid (**2**). As shown in Scheme 1, indole **5** was prepared from commercially available 4-hydrazinobenzoic acid,[26,22] and 3-methylbutan-2-one. Subsequent treatment with butanesultone led to indole-sulfonate **6**.[26,22] The reaction of the bis(dimethyl acetal) of propanedial with aniline, in aqueous **hydrochloric acid (**HCl) led to anilide **7** in 90% yield.[22] Subsequent reaction with indole derivative **6** in the presence of acetic acid/acetic anhydride buffered with sodium acetate gave a 30% yield of dye (**8)**.[22] We synthesized the dye-conjugate, **12**, from the non-targeted rigid dye, **8**, by coupling to the piperazine-2-nitroimidazole fragment (**11**), as shown in Scheme 2. Fragment **11** was prepared by

reaction of commercially available 2-nitroimidazole with ethyl bromoacetate to give **9**, followed by reaction with N-Boc piperazine to give **10**.[22] The coupling agent Pybop, (benzotriazol-1-yloxy) tripyrrolidinophosphonium hexafluorophosphate, was used in dimethylformamide (DMF) for the reaction of **8** with **11**, and final purification of the crude product on C18 reversed phase automated flash column chromatography gave **12** in 31% yield.

Preparation of 12.

Sodium 4-[2-[(1*E*,3*E*,5*Z*)-7-[1,1-dimethyl-3-(4-sulfonatobutyl)indol-2-ylidene]penta-1,3-dienyl]-1,1-dimethylindol-3-ium-3-yl]butane-1-sulfonate, 8.

A vigorously stirred solution of 3-(5-carboxy-2,3,3-trimethyl-3*H*-indolium-1-yl)propane-1-sulfonate (**6**, 0.14 g, 0.41 mmol) and **7** (0.05 g, 0.19 mmol) in acetic anhydride (1 mL) and acetic acid (0.5 mL) was treated with sodium acetate (0.054 g, 0.66 mmol) and heated at reflux (120 °C) for 45 min. The reaction mixture was cooled to ambient temperature and anhydrous diethyl ether (5 mL) was added. The resulting precipitate was isolated by vacuum filtration to give a crude solid that was recrystallized (methanol: water) to give **8** as a blue solid (0.09 g, 0.12 mmol, 63%);[22] mp: decomposition at 287 °C; ^{1}H NMR (400 MHz, CD_3OD) δ 12.92 (bs, 2H), 8.43 (t, *J* = 13 Hz, 2H), 8.17 (s, 2H), 8.00 (d, *J* = 8.4 Hz, 2H), 7.53 (d, *J* = 8.4 Hz, 2H), 6.71 (t, *J* = 12.4 Hz, 1H), 6.50 (d, *J* = 13.7 Hz, 2H), 4.15 (bs, 4H), 1.18-1.76 (m, 8H), 1.73 (s, 12H); ^{13}C NMR (100 MHz, CD_3OD) δ 175.7, 169.2, 156.8, 147.4, 142.8, 132.3, 128.7,128.6, 124.6, 112.0, 106.0, 51.7, 50.4, 45.1, 27.9, 27.2, 23.5; ^{13}C NMR (100 MHz, MeOD) d 175.7, 169.2, 156.8, 147.4, 142.8, 132.3, 128.7128.6, 124.6, 112.0, 106.0, 51.7, 50.4, 45.1, 27.9, 27.2, and 23.5 ppm. HRMS (TOF): [M+H]+ Calc'd for $C_{35}H_{43}N_2O_{10}S_2$ *m/z* 715.2359. Found, *m/z* 715.2321.

Sodium 4-((*Z*)-2-((2*E*,4*E*)-5-(3,3-dimethyl-5-(4-(2-(2-nitro-1*H*-imidazol-1-yl)acetyl)-piperazine-1-carbonyl)-1-(4-sulfonatobutyl)-3*H*-indol-1-ium-2-yl)penta-2,4-dien-1-ylidene)-3,3-dimethyl-5-(4-(2-(2-nitro-1*H*-imidazol-1-yl)acetyl)piperazine-1-carbonyl)indolin-1-yl)butane-1-sulfonate, 12.

A total of 78 mg (0.149 mmol) of PyBOP was added to a stirring solution of bis-(carboxylic acid) **8** (50 mg, .0068 mmol) in dry DMF (2 mL) at 0 °C. This solution was subsequently treated with HOBt (hydroxybenzotriazole, 20 mg, 0.149 mmol), followed by diisopropylethylamine (DIPEA, 0.026 mL, 0.149 mmol). This mixture was stirred for 15 min before the addition of 2-nitroimidazole piperazine **11** (54 mg, 0.149 mmol) followed by stirring at room temperature for 48 h in the dark. The DMF was removed by air-drying to yield a thick blue oil and further concentrated *in vacuo* overnight. The crude mixture was recrystallized from methanol (15 mL) via the dropwise addition diethyl ether (50 mL), and the resulting blue solid was washed with acetonitrile (2x25 mL), ethyl acetate (2x25 mL), and chloroform (2x25 mL). The crude was purified by C18 reverse phase column chromatography (H_2O:MeOH) to yield **12** (25 mg, 0.021 mmol, 31%) as a blue solid; mp: decomposed to black residue > 250 ^{o}C; ^{1}H NMR (400 MHz, D_2O) d 8.17 (m, 3H), 7.71 (s, 2H), 7.63 (d, J = 8 Hz, 2H), 7.55 (s, 2H), 7.50 (d, J = 8, 1H), 7.38 (s, 1H), 6.76 (t, 2H), 6.47 (d, 2H), 5.64 (bs, 4H), 4.27 (bs, 4H), 3.66-4.05 (bs, 16H), 3.06 (t, 4H), 2.10 (m, 4H), 1.97 (m, 2H), 1.80 (bs, 9H), 1.44 (m, 3H); HRMS (ESI-TOF): [M-Na]- Calc'd for *m/z* $C_{53}H_{63}N_{12}O_{14}S_2$ 1155.4034. Found, *m/z* 1155.4028.

Repeated efforts to obtain the ^{13}C NMR failed to give a spectrum. We observed this problem with dye conjugate **4**.[18] Although the dye (**2** and **8**) showed reasonable ^{13}C NMR spectra, **4** and **12** did not. We examined the possibility of aggregation, rotamers, relaxation time, and low concentration due to solubility issues. All of these issues can lead to poor ^{13}C NMR spectra. Attempts to obtain ^{13}C NMR spectra at 25 °C failed, and

we heated the samples to 55 °C to promote deaggregation. We also explored different solvents, including CD_3OD, $(CD_3)_2CO$, D_2O. We examined extended delay (relaxation) times up to 10 to 15 sec, as well as long acquisition times (up to 12 hours). None of these experiments led to a ^{13}C NMR. We have attempted indirect C^{13} experiments, including HSQC, HMBC, and CIGAR. The problem is likely due to low solubility of **4** and **12**, coupled with the low isotope percentage of ^{13}C relative to ^{12}C versus the high percentage of ^{1}H, but we do not have a definitive answer to this problem. No experiments have been successful, so only ^{1}H NMR data is provided.

Measurement of quantum yield

In order to measure the quantum yield of hypoxia-targeted rigid dye **12** and non-targeted rigid dye **8,** we followed the procedures described in the reference.[27] Any of these four unknown samples is measured against a fluorescence standard, Indocyanine green (ICG) from Sigma-Aldrich with a known quantum yield Φ_f=0.012[28] with Varian Cary® 50 UV-Vis Spectrophotometer and Varian Cary® Eclipse Fluorescence Spectrophotometer. The fluorescence quantum yield is then calculated according to equation 1, by taking into account the absorbance through the absorption factor $f_x(\lambda_{ex})$ and the fluorescence through the integral of fluorescence $F^x(\lambda_{em})$ at specific excitation wavelength λ_{ex} and a range of collection wavelength band λ_{em}.

$$\Phi_f^i = \Phi_f^s \frac{f_s(\lambda_{ex})}{f_i(\lambda_{ex})} \frac{\int_{\lambda_{em}} F^i(\lambda_{em})}{\int_{\lambda_{em}} F^s(\lambda_{em})} \quad (1)$$

Here both standard (s) and unknown dye (i) were measured in 9.25% sucrose, thus compared with the reference, the difference of refractive indices between standard and unknown dye can be ignored. The excitation/collection wavelengths are shown in Figure 2.

Murine tumor model and imaging

Murine tumor model preparation procedures have been reported previously.[18] The procedures were performed in accordance with specifications in animal protocol approved by the Institutional Animal Care and Use Committee of University of Connecticut. Six to Eight week old balb/c mice with body weight around 20g were used in this study and transplanted with 4T1 tumor cells. The experiments were performed when the tumor size had attained a diameter of 5 mm or greater, 10-15 days post-inoculation. Mice with a tumor bared on the top of their right legs were imaged with an IVIS® Lumina II Imaging System (Caliper Life Sciences, Hopkinton, MA).[29]

Mice were separated into four groups with same average tumor size. Each group of mice was injected, via retroorbital injection, with 100 µl of either biscarboxylic acid ICG (**2**), piperazine-2-nitroimidazole-ICG (**4**), non-targeted rigid dye (**8**), or hypoxia-targeted rigid dye (**12**) at a concentration of 25 µM.

Imaging the tumors began 1 minute post-injection and were repeated at 15 min, 30 min, 1, 2, 3, 4, 5, 6, 7, 8, 9, 10, 24 and 48 h. In all cases, the *in vivo* fluorescence intensity was quantified. After 48 h, the tumor tissue were excised from each sacrificed mouse, and immediately frozen in the liquid nitrogen. After acquiring florescence images, the tissues were stored in the -80 °C freezer for later histology processing.

Immunohistochemistry

To visualize the hypoxic area in the tumor samples by immunohistochemistry (IHC), the Hypoxyprobe™1 plus kit,

which contains the 2-nitroimidazole derivative pimonidazole hydrochloride [1-(2-nitro-1*H*-imidazol-1-yl)-3-(piperidin-1-yl)propan-2-ol] was purchased from HPI, Inc. (Burlington, Massachusetts, USA). A total of 60 mg of pimonidazole hydrochloride per kg body weight, diluted in 0.9% saline solution was injected intravenously into mice 30-45 minutes before sacrificing. Immediately after the animals were euthanized, the tumor specimens were collected and flash-frozen in the liquid nitrogen, and subsequently sectioned into 16 µm sections on a Leica CM 3050S cryotome (Leica, Nussloch, Germany). The prepared tumor sections (sample number: 8 for hypoxia-targeted rigid dye, 12 for non-targeted rigid dye) were stored in -80 °C before staining. After thawing, the sections were fixed in cold acetone for 10 minutes, and later rinsed and incubated overnight at 4 °C with FITC-Mab1 diluted 1:20 in PBS containing 0.1% bovine serum albumin and 0.1% Tween 20.

The hypoxic areas were visible with FITC attaching to pimonidazole hydrochloride under the fluorescence microscope (Zeiss Axio M2, Pennsylvania, USA). In order to analyze the targeting property of **12** in tumor, fluorescence images are acquired simultaneously with filter sets for channel 1- Cy5 and channel 2- FITC. The absorption and emission peaks of Cy5 (650/670 nm respectively) are overlapped with that of **12** and **8**. Digital images of the whole tissue slices were scanned and acquired with 2.5× and 10× objective magnifications. For 10× magnification, the exposure time is used as 1200 ms for channel 1 and 250 ms for channel 2. Obtained digital images were transferred to ImageJ software, delineated with the boundaries of hypoxic areas, split by channels for separate analysis. Each image is later imported to Matlab, converted into a binary image with a threshold of 12% of the labelled tissue area, and used for computing the correlation of the labelled areas between pimonidazole hydrochloride and the rigid dye (**12** or **8**).

Conclusions

. Hypoxia is an important tumor microenvironment and targeting tumor hypoxia is significant in predicting tumor response to treatments. Our *in vivo* experimental results of the third generation tumor hypoxia-targeting fluorescence dye, **12**, showed that it exhibited superior fluorescence detectability for hypoxic tumors *in vivo*. The fluorescence quantum yield of **12** was measured to be ~0.467, which is about 5 times higher than the 0.083 measured for the second-generation hypoxia dye (**4**). Experiments on mice showed that **12** provided more than twice the fluorescence intensity in tumors 2 hours post-injection as compared with the second-generation hypoxia dye (**4**). Our results suggest that **12** may significantly improve *in vivo* detection of tumor hypoxia beyond this initial study

Acknowledgements

The authors acknowledge Connecticut Public Health and NIH R01002136 for partial funding of this project. We thank Prof. Xiuling Lu and Donghui Song, UConn School of pharmacy, for allowing us to use their laboratory for maintaining 4T1 tumor cell line. The University of Connecticut Animal Care and Use Program is accredited by AAALAC International.

References

1 P. Vaupel, A. Mayer *Cancer Metast. Rev.,* 2007*,* **26**, 225-239.
2 M.C. Brahimi-Horn, and J. Chiche, J. Pouysségur *J. Mol. Med.,* 2007*,* **85***,* 1301-1307.
3 P. Vaupel and F. Kallinowski, P. Okunieff *Cancer Res.,* 1989*,* **49**, 6449-6465.
4 J.M. Brown and W.R. Wilson *Nat. Rev. Cancer,* 2004**,** **4***,* 437-447.

5 W.R. Wilson and M.P. Hay *Nat. Rev. Cancer,* 2011*,* **11**, 393-410.
6 M. Höckel and P. Vaupel *J. Natl. Cancer Inst.,* 2001*,* **93***,* 266-276.
7 E. Hammond, M.-C. Asselin, D. Forster, J. O'Connor, J. Senra, and K. Williams *Clin. Oncol.,* 2014*,* **26**, 277-288.
8 A. Nunn, K. Linder, and H.W. Strauss *Eur. J. Nuc. Med.,* 1995*,* **22**, 265-280.
9 L. Mei, Y. Wang, and T. Chu *Eur. J. Med. Chem.,* 2012*,* **58**, 50-63.
10 H. Huang, H. Zhou, Z. Li, X. Wang, and T. Chu *Bioorg. Med. Chem. Lett.,* 2012*,* **22**, 172-177.
11 L.-B.-A. Tran, A. Bol, D. Labar, B. Jordan, J. Magat, L. Mignion*,* V. Grégoire, and B. Gallez *Radiother Oncol.,* 2012*,* **105***,* 29-35.
12 Z. Li and T. Chu *Curr. Pharm. Des.,* 2012*,* **18**, 1084-1097.
13 Z. Guo, S. Park, J. Yoon, and I. Shin *Chem.Soc. Rev.,* 2014*,* **43**, 16-29.
14 A. Corlu, R. Choe, T. Durduran, M.A. Rosen, M. Schweiger, S.R. Arridge, M.D. Schnall, and A.G. Yodh *Opt. Express,* **2007***,* **15**, 6696-6716.
15 M. Aldrich, C. Davies-Venn, B. Angermiller, H. Robinson, W. Chan, S. Kwon, and E.M. Sevick-Muraca *Lymphat Res Biol.,* 2012*,* **10***,* 20-24.
16 N.C. Biswal, C. Pavlik, M.B. Smith, A. Aquirre, L.T. Kuhn, Y. Xu, S. Zanganeh, L.T. Kuhn, K.P.; Claffey, and Q. Zhu, *J. Biomed. Opt.,* 2011*,* **16(6),** 066009-01 - 066009-08.
17 C. Pavlik, N.C. Biswal, F.C. Gaenzler, M.D. Morton, L.T. Kuhn, K.P. Claffey*,* Q. Zhu, and M.B. Smith *Dyes Pigments,* 2011*,* **89**, 9-15.
18 Y. Xu, S. Zanganeh, I. Mohammad, A. Aguirre, T. Wang, Y. Yang, M.B. Smith, and Q. Zhu *J. Biomed. Optics,* 2013*,* **18(6)**, 066009-1-11.
19 S. Zanganeh, F. Zhou, A. Abuteen, I. Mohammad, M.B. Smith, and Q. Zhu *Biomedical Optics*, 2014, p. BT3A. 51. Conference presentation**.**
20 N. Nijegorodov and W. Downey *J. Phys. Chem.,* 1994*,* **98**, 5639-5643.
21 H. Suzuki, *Bull. Chem. Soc. Jpn., 1959,* **32**, 1340-1350.
22 I. Mohammad, C. Stanford, M.D. Morton, Q. Zhu, and M.B. Smith, *Dyes Pigments, 2013,* **99**, 275-283.
23 O. Mazuryk, M. Maciuszek, G. Stochel, F. Suzenet, and M. Brindell *J. Inorg. Biochem.,* 2014*,* **134**, 83-91.
24 K. Okuda, Y. Okabe, T. Kadonosono, T. Ueno, B.G. Youssif, S. Kizaka-Kondoh, and H, Nagasawa *Bioconjugate Chem.,* 2012*,* **23**, 324-329.
25 J. Pauli, U. Resch-Genger, W.A. Kaiser, I. Hilger, F.M. Hamann, R. Brehm, M. Grabolle, W. Frank, and D. Fischer *Mol. Imaging,* 2011*,* **10**, 258-269.
26 E. Jung and W.-J. Kim *Biorg. Ed. Chem.,* 2006*,* **14**, 92-97.
27 M. Grabolle, M. Spieles, V. Lesnyak, N. Gaponik, E. Alexander, and U. Resch-Genger *Anal. Chem.,* 2009*,* **81***,* 6285-6294.
28 R. Reisfeld *Le Journal de Physique Colloques,* 1987*,* **48(C7),** *C7-423-C7-426*.
29 S.K. Cool, K. Breyne, E. Meyer, S.C. De Smedt, and N.N. Sanders *J. Fluoresc.* 2013*,* **23**, 909-920.